Field Crops Research 127 (2012) 51–63

Contents lists available at SciVerse ScienceDirect

Field Crops Research

journal homepage: www.elsevier.com/locate/fcr

Biophysical characteristics of maize pollen: Variability during emission and consequences on cross-pollination risks

Alexis Marceau[a,b,c,*], Sébastien Saint-Jean[a,c], Benjamin Loubet[a,c], Xavier Foueillassar[b], Laurent Huber[a,c]

[a] INRA UMR 1091 Environnement et Grandes Cultures, Thiverval-Grignon, France
[b] Arvalis – Institut du végétal, Montardon, France
[c] AgroParisTech UMR 1091 Environnement et Grandes Cultures, Thiverval-Grignon, France

ARTICLE INFO

Article history:
Received 9 December 2010
Received in revised form 5 August 2011
Accepted 3 November 2011

Keywords:
Zea mays
Pollen
Emission
Settling velocity
Viability
Dehydration

ABSTRACT

Modelling of cross-pollination risks using physical-based model of pollen dispersal requires estimations of pollen viability rate as well as settling velocity distribution of viable pollen grains at emission. These two biophysical characteristics are mainly determined by pollen water content. Three years of experiments were carried out to measure biophysical characteristics of pollen at different times of emission within the day. In a first part, we proposed a simple model to predict pollen water content at emission as a function of air vapour pressure deficit. We found that by setting a constant duration of pollen dehydration in the anthers the model predicts accurately pollen water content variations at emission. In a second part, we related pollen water content and settling velocity distribution of viable and non-viable pollen grains. We used with success settling velocity distribution as a proxy to estimate fraction of spheroid pollen, water content distribution of spheroid pollen and pollen viability rate. In addition, we validated with success the estimations of viability rate. In a third part, based on above models, we estimated the effects of air humidity on cross-pollination risks.

1. Introduction

Reducing both cross-pollination in hybrid seed production and out-crossing from genetically modified fields is an economic concern as well as a regulatory matter of how to ensure coexistence. For maize, physical processes of aerial pollen dispersal have been modelled (Aylor et al., 2003; Jarosz et al., 2005; Dupont et al., 2006; Arritt et al., 2007). Models could be used to predict quantities of maize pollen dispersed in a neighbouring maize field downwind from an emitting field to evaluate the potential for cross-pollination (Beckie and Hall, 2008). For inputs, these models require the quantity of pollen emitted, at a given time, as well as its settling velocity distribution. In order to quantify potential cross-pollination over the pollen emission period, current models need their inputs to be estimated over this same emission period. To this end, models of total pollen quantities released over the emission period, on an hourly basis, have been recently proposed by Marceau et al. (2011) and Viner et al. (2010). Total pollen quantity implies both dead and viable pollen, the latter being the fraction of pollen able to develop a tube dedicated to ovule fecundation. In the case of cross-pollination studies, the quantity of viable pollen alone would be a more relevant input than total quantity; however, to date, models do not account for the fraction of viable pollen. Moreover, from our knowledge, modelling of settling velocity distribution of viable pollen at the emission time over the emission period is not available.

Pollen water content determines many of the biophysical characteristics of pollen such as viability rate and settling velocity. From a morphological point of view, fully hydrated pollen is prolate spheroid whereas fully dehydrated pollen is prismatic (Luna et al., 2001). For eleven maize varieties, Fonseca and Westgate (2005) observed that the percentage of viable pollen decreases linearly with pollen water content and that the linear relationships were fairly similar between varieties. On average, a maximum percentage of 79% of viable pollen was measured, corresponding to water content of 60%. Null viability was reached when water content dropped to around 30%. On the contrary, for a given hybrid, Aylor (2004) found that the percentage of viable pollen does not decrease linearly with pollen water content. The percentage of viable pollen was maximal (65%) for water content higher than 30% and null

* Corresponding author at: INRA, Centre de Versailles-Grignon, UMR 1091 INRA – AgroParisTech Environnement et Grandes Cultures, 78850 Thiverval-Grignon, France. Tel.: +33 0 2 41 72 73 32; fax: +33 0 1 30 81 55 63.
E-mail addresses: marceau.a@gmail.com (A. Marceau), Sebastien.Saint-Jean@AgroParisTech.fr (S. Saint-Jean), benjamin.loubet@grignon.inra.fr (B. Loubet), x.foueillassar@arvalisinstitutduvegetal.fr (X. Foueillassar), laurent.huber@grignon.inra.fr (L. Huber).

0378-4290/$ – see front matter © 2011 Elsevier B.V. All rights reserved.
doi:10.1016/j.fcr.2011.11.006

for water content below 5%. Mean settling velocity was found to vary from 17 to 32 cm s^{-1} for totally dehydrated and fully hydrated pollen, respectively (Aylor, 2002; Loubet et al., 2007).

For several samples of pollen collected in the field, Loubet et al. (2007) found a bimodal distribution of pollen settling velocity suggesting a mixture of pollen with two different aerodynamic properties. They suggest that hydrated and dehydrated pollen are mixed. Indeed, pollen water content affects pollen mass, diameter, and density. These properties in turn determine pollen settling velocity as formulated by Di-Giovanni et al. (1995). Pollen mass was found to range from 0.2 to 0.7 μg per grain whose diameter was found to range from 76–80 μm to 103–106 μm for fully dehydrated and fully hydrated pollen grains, respectively (Aylor, 2002; Jarosz, 2003). Pollen density therefore ranged from 1.45 to 1.25 g cm^3 for dry and hydrated grains, respectively (Aylor, 2002). However, van Hout and Katz (2004) measured lower density values of 1.14 and 1.11 g cm^3 for dry and hydrated pollen grains, respectively. They explained this discrepancy by the pycnometer measurements used by Aylor (2002) which measure the density of the solid portion of pollen without its gas pockets. They estimated that air represents about 24% of the dry volume.

Variability of pollen water content as a function of emission time was studied by Fonseca and Westgate (2005) who reported that pollen water content at emission was fairly stationary, around 57%, during the initial hours of pollen emission within the day. Westgate and Boyer (1986) reported that the water potential of pollen at emission decreased depending on the time of emission during the day: the decrease was small for an emission between 0800 and 15:00 UTC and stronger for an emission between 1500 and 18:00 UTC. They suggested that there is a time gap between anther dehiscence (air entrance into the anther) and pollen release but did not quantify it. This could explain pollen grain dehydration throughout the day by the increase in vapour pressure deficit that also occurs throughout the day. Pollen dehydration in the anther is possible: Keijzer et al. (1996) have observed that the helix layout of pollen in anthers leaving an empty space over the central axis allowing water exchange between air and all pollen grains after anther dehiscence.

Pollen dehydration has been well studied during pollen travel in the atmosphere after emission (Aylor, 2004; Shivanna and Heslopharrison, 1981). Exposed to air, pollen grains constantly dehydrate until total dehydration or landing on a stigma where they rehydrate (Nepi et al., 2001). Aylor (2003) revealed that pollen grains were generally totally dehydrated in 1–4 h after their release depending on climatic conditions. In cool and moist environments, such as at elevated altitudes, pollen was seen to be preserved much longer from dehydration (Viner and Arritt, 2010). A model describing the relationship between pollen dehydration and vapour pressure deficit has been proposed by Fonseca and Westgate (2005). Through an exponential decay, it empirically relates pollen water content and cumulated vapour pressure deficit per minute from the beginning of dehydration. This equation has proved to be valid for several inbred lines and hybrids.

In this paper, we investigate and model pollen water content at emission time and consequences on settling velocity and viability rate of pollen. Our hypothesis is that vapour pressure deficit of the air does not only govern the dehydration of pollen while travelling in the air but also when it is in the anther, from the time of anther dehiscence until the pollen is emitted. This dehydration is supposed to decrease settling velocity and viability rate of pollen.

To model these effects, we propose two sub-models to predict at the emission time (i) the water content using a dehydration model of the literature (Fonseca and Westgate, 2005) and (ii) settling velocity distributions of viable and non-viable pollen grains as well as viability rate using original relationships with water content. Parameters of these models were estimated using experimental data collected over four emission periods using the same maize hybrid and providing hourly time course of water content, settling velocity distributions, diameter and shape of pollen grains. A second dataset collected in four maize hybrid fields with different varieties was used to validate estimations of viability rate at emission time. Finally, we simulate and then discuss the role of vapour pressure deficit on pollen water content at emission and the consequences on settling velocity and shape distribution, viability rate as well as cross-pollination risks.

2. Material and methods

2.1. Experimental data for model parameter estimations

2.1.1. Experimental design

Climatic data and biophysical pollen characteristics were recorded over four pollen emission periods in maize fields grown in Thiverval-Grignon (France, 48°51′N, 1°55′E, 101 m) in 2008 and 2009. Each year, the hybrid variety Meribel was sown in two plots at dates spaced three weeks apart (25 April and 13 May in 2008 and 24 April and 19 May in 2009). This ensured lagged flowering periods under different climatic conditions. The area of the plots was around 0.5 ha. Rows were spaced 80 cm apart. The density was 95,000 plants/ha. Plots were located near the laboratory to reduce the delay between pollen collection and pollen measurements.

For each pollen emission period the following meteorological data were measured: relative humidity, rainfall, water vapour pressure, surface wetness, wind speed and direction, temperature, and global radiation. These measurements were taken every 5 s and averaged over successive 15 min intervals. Global radiation and wind measurements were recorded at 5 m height while other variables were measured at tassel height.

2.1.2. Measurements of pollen characteristics at different times of emission during the day: settling velocity, diameter, shape, and water content

For each emission period, pollen characteristics were measured when the quantities of pollen emitted were maximal. Measurements began when more than 50% of the plants was emitting pollen and were taken for the following 5–6 days. Every 2 h between 08:00 and 16:00 UTC a sample of pollen was collected by gently shaking 10–20 tassels along a same row. At each collection a different row was randomly chosen. To collect the maximum of pollen grains, tassels were shaken above a cardboard folded in half and tilted to 45°. Pollen grains slide along the fold and settle in an aluminium container. When all tassels have been shaken the aluminium container was closed and then enclosed in a bigger plastic container to prevent dehydration. Pollen grains were released from opened anthers and were supposed to be representative of pollen emitted at this time at the field scale.

Within the 10 min following collection, four biophysical characteristics of each sample were assessed using a distribution or a mean value: settling velocity (distribution), shape and diameter (distribution), and water content (mean). In a few cases, the quantity of pollen was not sufficient to measure all characteristics (often at 12:00 and 14:00 UTC) for which only diameter and shape distributions were measured.

In addition to these pollen samples collected at emission, to assess the four biophysical characteristics for highly dehydrated pollen, an extra sample of pollen was naturally dried in the laboratory for a day (referred throughout the paper as the pollen sample dried in the laboratory).

The distribution of settling velocity was assessed using a "settling tower" developed by Loubet et al. (2007). Briefly, at the top of a 1 m high tube, pollen grains were released continuously for at

least 1 min, falling down through still air due to gravity. At about 20 cm from the bottom of the tube, falling pollen was photographed with a digital camera (15 pictures/s). Then, to estimate individual settling velocities, individual pollen grains were tracked by image analysis along the sequence of pictures, providing time and distance travelled. The number of pollen grains tracked ranged from 100 to 6000. Measurements with a number of pollen lower than 200 pollen grains were not taken into account.

The distributions of shape and diameter were estimated from pictures taken from the microscope and image analysis. A microscope slide was powdered with pollen and placed under a light microscopy (no oil and cover-slip were used). Pollen was illuminated (with a fixed luminosity) and 10 pictures were taken from the left to the right side (resolution of 1.25 μm per pixel). This represents a total number of 200 ± 60 pollen grains. For each individual pollen grain on each picture, the projected area and perimeter were estimated by image analysis, with ImageJ software (Saint-Jean et al., 2005). The analysis entails splitting the red channel of the picture (where pollens grains contrasted the most with background) into pollen and background using IsoData algorithm (Rasband, 1997–2009). This algorithm automatically estimated a threshold of grey intensity around which pixels are attributed to pollen or background. Then, individual pollen grains were located and their projected areas were estimated. Based on these estimations, equivalent circular diameters (D_p) were calculated as the diameters of the circles that have areas equivalent to individual pollen grains (Eq. (1)).

$$D_p = 2 \times \sqrt{\frac{\text{area}_p}{\pi}} \quad (1)$$

We also calculated the kurtosis of grey intensity distribution within individual pollen, K_p, which has been observed to effectively discriminate spheroid and prismatic pollen. Spheroid pollen has a homogeneous colour contrasting with background. On the contrary, prismatic pollen is bicoloured: one colour corresponds to the pollen and the other to the background. Indeed, prismatic pollen has depressions on its surface thought which the background is visible by transparency. Thus, the grey intensity distribution is flat for prismatic pollen while it is more peaked for spheroid pollen.

Mean relative water content of pollen grains was calculated as the water mass divided by the fresh mass (i.e., water mass plus dry mass) of the pollen sample. Masses were obtained using a micro balance (Sartorius AG, Göttingen, Germany, resolution 10^{-6} g). Total pollen mass was measured from a pollen sample of around 10–50 mg. Dry mass was obtained by drying the pollen sample in a drying oven set at 80 °C for 15 min. Water mass was assumed to be the difference between total and dry mass. For each pollen collection, three repetitions were used and the mean value was calculated.

In addition to these measurements, the mean dry mass of individual pollen grain (m_{dry}) was estimated for the five samples of pollen collected over the day (2009-07-29). First, pollen samples were dried and the total dry mass was measured. Second, the number of pollen grains in each sample was estimated using an automatic counter apparatus based on volumetric detection (Coulter Multisizer III, Beckman, USA).

2.2. Experimental data for validation of viability rate estimations

Pollen viability rate at emission time was measured within maize hybrid fields between 15th July and 1st August 2010 near Beaufort-en-Vallée in the west of France (47°26′N; 0°12′O). Four isolated farmer fields were selected localized at distances lower than 25 km from the laboratory and from a national meteorological station.

Viability rates of pollen at emission time were measured in vitro using germination medium disposed within maize fields during several hours. Germination medium were stocked in Petri dishes and were composed of saccharose (120 g/l), $CaCl_2$ (300 mg/l), H_3BO_3 (100 mg/l) and agar (10 g/l) (produced by Arvalis-Institut du vegetal according to Fonseca and Westgate (2005)).

Starting between 08:00 and 10:00 UTC, a set of three Petri dishes were placed within fields and opened during 2–4 h before being replaced by three new Petri dishes. For a given day and a given field, a maximum of three replacements was realized. Petri dishes were pasted at the top of 1 m height stacks driven into the ground between the 14th and the 15th maize rows from the downwind edge of the field. A total of 35 exposure periods over 11 days was realized. Within the three next days following the exposure, the numbers of germinated and non-germinated pollen grains were counted at the laboratory. When a medium was not counted before the end of the day of its collection it was placed in the fridge to stop pollen tube growth and facilitate the counting. Pollen grains are considered as germinated when a tube is shown even if it is smaller than pollen diameter.

Meteorological conditions were recorded by a national station of Météo-France localized between 3 and 23 km from fields and at higher altitudes (between 4 and 24 m). The station measured at each hour the temperature, relative humidity, wind speed and direction.

2.3. Modelling of pollen water content at emission time

We assume that pollen grains dehydrate in the anther on contact with air from the time of anther dehiscence, i.e., when air enters the anther, until the time of actual pollen emission. This time interval is referred throughout the paper as the duration of dehydration. It is now well established that pollen dehydration rate is a function of vapour pressure deficit of the air (Aylor, 2003; Fonseca and Westgate, 2005). Knowing the vapour pressure deficit in the anther and the duration of dehydration, pollen water content at emission (W_p in %) could be calculated using the simple model of Fonseca and Westgate (2005):

$$W_p(\tau) = 63.2 \exp(-0.0012 \sum_{t=1}^{\tau} \text{VPD}_t) \quad (2)$$

where VPD_t is the vapour pressure deficit in the anther (mmHg) at the time t since the beginning of dehydration (min), τ, the duration of dehydration (min) and W_p the pollen water content at emission (%). In this equation, the initial pollen water content (at the beginning of dehydrating period, i.e., the anther dehiscence) was 63.2%.

To use this model, our work was dedicated to estimate VPD_t in the anther as well as the variable τ using Grignon experimental data. First, we assumed the same conditions of VPD_t in the anther as in the air at the tassel height. Second, for each pollen collection, we estimated the duration of dehydration τ, leading to the measured mean water content by using the inverse function of Eq. (2) and the measured air vapour pressure deficit at the tassel height. For each measurement of mean water content, inverse function of Eq. (2) provided the corresponding cumulated vapour pressure per minute required. By cumulating the vapour pressure deficit measured before the pollen collection we estimated the duration of dehydration associated to the measured mean water content. Then, we explored relationships between τ and mean climatic conditions within the duration of dehydration.

2.4. Pollen dehydration consequences on settling velocity distribution and viability rate

2.4.1. Relationships between water content and settling velocity distribution

Pollen water content determines diameter, mass and shape and in turn pollen settling velocity. Using experimental data collected in Thiverval-Grignon, empirical relationships between mean water content and settling velocity distribution were estimated. To ensure that measured settling velocity distributions corresponded to a sufficient pollen sample size we defined classes of water content and pooled together the measured settling velocities corresponding to the same class. Sixty classes of water content were defined between 0% and 60% by step of 1%. For each class of water content, associated settling velocity distribution, $f_{v_S}(v_S)$, was approximated by a sum of two Gaussian distributions as proposed in Loubet et al. (2007).

$$f_{v_S}(v_S) = \frac{(1-A_2)}{\sqrt{2\pi}\sigma_1} \exp\left(-\frac{(v_S-\mu_1)}{2{\sigma_1}^2}\right) + \frac{A_2}{\sqrt{2\pi}\sigma_2} \exp\left(-\frac{(v_S-\mu_2)}{2{\sigma_2}^2}\right) \quad (3)$$

where v_S is the settling velocity ($m\,s^{-1}$) and μ_1, μ_2 and σ_1, σ_2 are the mean and standard deviations ($m\,s^{-1}$) of the two Gaussian distributions. A_2 is the area under the second Gaussian distribution curve assuming a total area equal to 1. Parameters were estimated by minimizing errors with the measured distributions of settling velocity using the least square method. Then, empirical relationships between the five parameters and mean water content were estimated using weighted least square methods. A linear relationship was chosen for σ_1, σ_2 and A_1 while a sigmoid function was chosen for μ_1, μ_2 after plotting the results. Weights were equal to the pollen sample size associated to each distribution of settling velocity. Using the estimated bi-Gaussian distribution, we calculated the threshold of settling velocity around which the two Gaussian distributions are split. It was calculated as the average between 95% quantiles of the Gaussian distribution associated to the highest settling velocity and 5% quantiles of Gaussian distribution associated to the lowest settling velocity.

To understand if the bimodal settling velocity distribution resulted from a mixture of either contrasted diameters or spheroid and prismatic shapes, we explored the corresponding distributions of diameter and kurtosis of grey intensity, K_p. First we plotted diameter and K_p distributions as a function of water content and observed if they have a bimodal distribution. For K_p, we estimated a threshold value around which pollen grains could be considered as spheroid or prismatic. Two series of pictures were chosen with only spheroid pollen or only prismatic pollen. Then, a K_p threshold around which pollen is prismatic or spheroid was deduced. Using this threshold proportion of spheroid and prismatic pollen was estimated and compared to proportion of each Gaussian distribution of settling velocity.

2.4.2. Settling velocity distributions of viable and non-viable pollen

Because water content determines both viability and settling velocity, settling velocity of viable pollen and non-viable pollen are different. We relate corresponding fraction of viable and non-viable pollen to two settling velocity distributions. To this end, we assumed that a given water content correspond to a given settling velocity and a given viability rate without taken into account other variability. Thus, the bimodal settling velocity distribution was supposed to be the result of water content variability. Water content variability was assessed by developing a theoretical relationship between settling velocity and water content for spheroid pollen. This was based on the equation of settling velocity for spherical particle falling in still air given by Aylor (2002):

$$v_S^2 = \frac{4g}{3\rho_a} \times \frac{\rho_p D_p}{c_d(v_S, D_p)} \quad (4)$$

where the constants are the gravity ($g = 981\,cm\,s^{-2}$) and the air density ($\rho_a = 0.00127\,g\,cm^{-3}$). The variables are the pollen density (ρ_p in $g\,cm^{-3}$), the pollen diameter (D_p in cm) and the drag coefficient (c_d) depending on v_S ($cm\,s^{-1}$). The settling velocities were calculated by numerically solving the equation of motion with Runge–Kutta fourth order technique (Saint-Jean et al., 2004).

To express settling velocity as a function of water content we expressed density and diameter as functions of water content in the Eq. (4). We proposed a theoretical density using pollen mass estimated by Eq. (5) and using pollen volume estimated by Eq. (6). Mass of pollen grains (m_p in g) was estimated from measured water content as:

$$m_p = \frac{m_{dry}}{(1 - W_p/100)} \quad (5)$$

where m_{dry} is the dry mass of pollen (g), supposed to be constant and measured during the experiments and W_p the pollen water content (%).

Pollen volume (V_p in cm^3) was calculated by defining a standard turgescent pollen characterized by a reference diameter (D_{ref}) and a reference water content (W_{ref}, Eq. (6)) which could be estimated from measurements. V_p is calculated as the volume of standard turgescent pollen, calculated using D_{ref} and assuming spherical shape (first term of Eq. (6)), minus the volume of water evaporated (second term of Eq. (6)). The volume of water evaporated was calculated using its mass given by the difference between reference mass and actual pollen mass calculated using Eq. (5).

$$V_p = \frac{\pi D_{ref}^3}{6} - \frac{m_{dry}}{\rho_{H_2O}} \times \left(\frac{1}{1 - W_{ref}/100} - \frac{1}{1 - W_p/100}\right) \quad (6)$$

where D_{ref} and W_{ref} are the reference diameter (cm) and reference water content (%) of standard turgescent pollen. D_{ref} and W_{ref} were provided by experimental measurements. ρ_{H_2O} is the water density ($1\,g\,cm^{-3}$). This expression provided volume used for density calculation and also for diameter calculation. Diameter was calculated as an equivalent diameter of a spherical particle with a volume V_p.

To validate the theoretical relationship, we compared it with previously published theoretical relationship. Aylor (2002) proposed a theoretical relationship between settling velocity and diameter by expressing pollen density in Eq. (4) by:

$$\rho_p = \rho_{H_2O}\left[1 - \left(\frac{D_{dry}}{D_p}\right)^3\right] + \rho_{dry}\left(\frac{D_{dry}}{D_p}\right)^3 \quad (7)$$

where D_{dry} and ρ_{dry} are the diameter (given by measurements) and density of a fully dehydrated pollen grain. D_{dry} equal to 78 μm as given by Aylor (2002). Two values of ρ_{dry} founded in the literature, $1.14\,g\,cm^3$ (van Hout and Katz, 2004) and 1.45 (Aylor, 2002), were tested against empirical density. We also used empirical density to validate our theoretical densities. Empirical density was estimated by dividing mass by volume calculated using the measurements of diameter and of water content. Pollen volumes (V_p) were calculated from diameter assuming a spherical shape of pollen.

To estimate the distribution of settling velocity of viable and non-viable pollen, we calculated the water content distribution of spheroid pollen grains, $f_{W_p}(W_p)$, from their settling velocity distribution, $f_{v_S}(v_S)$, by a change of variable using Eq. (8).

$$f_{W_p}(W_p) = \left|\frac{1}{I'(I^{-1}(W_p))}\right| f_{v_S}(I^{-1}(W_p)) \quad (8)$$

where $I(v_S)$ and $I^{-1}(W_p)$ represent the inverse relationship and the relationship between settling velocity and water content, respectively. $I'(v_S)$ is the derived function of $I(v_S)$. $I(v_S)$ was estimated by adjusting an empirical function between water content and estimated theoretical settling velocity from Eqs. (4) to (6). An empirical function was used rather than the theoretical relationship to obtain analytic solutions of $I^{-1}(W_p)$ and $I'(v_S)$.

Assuming that pollen is irreversibly unable to germinate when its water content decreases below a threshold noted W_{dead}, we calculated settling velocity value corresponding to W_{dead} noted $v_{s,dead}$. Settling velocities of spheroid pollen higher than $v_{s,dead}$ correspond to viable pollen while lower settling velocities correspond to non-viable pollen. W_{dead} was calculated using the empirical equation of Fonseca and Westgate (2005) (Eq. (9)) which has been validated with success for several hybrid maize varieties ($R^2 = 0.86$).

$$R_p = -78 + 2.6W_p \quad (9)$$

where R_p is the viability rate (%) and W_p the mean water content (%). This equation gives a W_{dead} equal to 30%.

The viability rate is calculated by multiplying (i) the fraction of spheroid pollen, (ii) the fraction of potentially viable spheroid pollen, calculated as the fraction of settling velocities higher than $v_{s,dead}$ and (iii) initial fraction of defective pollen. Initial fraction of defective pollen was calculated using Eq. (9) using measured W_p in pollen sample with only spheroid pollen grains.

2.4.3. Comparison between measured and estimated pollen viability rate

Comparison between measured and estimated viability rate at emission time was performed using experimental data collected in Beaufort-en-Vallée in 2010. Hourly measurements of relative humidity and temperature recorded by a station of Météo-France were used to calculate hourly air vapour pressure deficit (VPD) (Hatfield and Baker, 2005). VPD was interpolated each minute for each field by assuming stationary during successive 1 h interval and equivalent on each maize field. Using VPD per minute and the model described above, viability rate was estimated each minute over the experimental period. Then, mean viability rate during each period of medium exposure were calculated. A weighted mean was calculated using estimation of pollen emission per minute divided by the total emission during the germination medium exposure period. Pollen emission per minute was estimated using the model of Marceau et al. (2011). We compared estimations with each measurement using the median measured viability rate among the three repetitions. We calculated the mean absolute error (MAE) to provide the accuracy of the model.

2.5. Simulation of air humidity effects on cross-pollination risks

To understand the effects of VPD on cross-pollination risks, we firstly estimated mean settling velocity of viable pollen and viability rate for VPD varying between 0 and 3000 Pa. They were estimated using model predicting pollen water content as a function of VPD and empirical relationships between water content and bi-Gaussian parameters of settling velocity.

Secondly, we simulated deposition of viable and non-viable pollen downwind from a 100 m long emitting field. Three conditions of vapour pressure, 1100, 2200 and 3300 Pa, and two conditions of wind speed, 1 and 5 m s^{-1}, were studied. Firstly, we estimated mean water content at emission using Eq. (2) for the three conditions of vapour pressure deficit. Secondly, using the estimated mean water content, we calculated the settling velocity distribution of viable and non-viable pollen as well as viability rate from the empirical relationships estimated previously. Thirdly, these estimations were used as input of a physical-based Lagrangian model (Jarosz et al., 2004) to simulate deposition of viable and non-viable pollen downwind the emitting field. The outputs of the simulations provide the fraction of viable pollen deposited at several distances downwind the field.

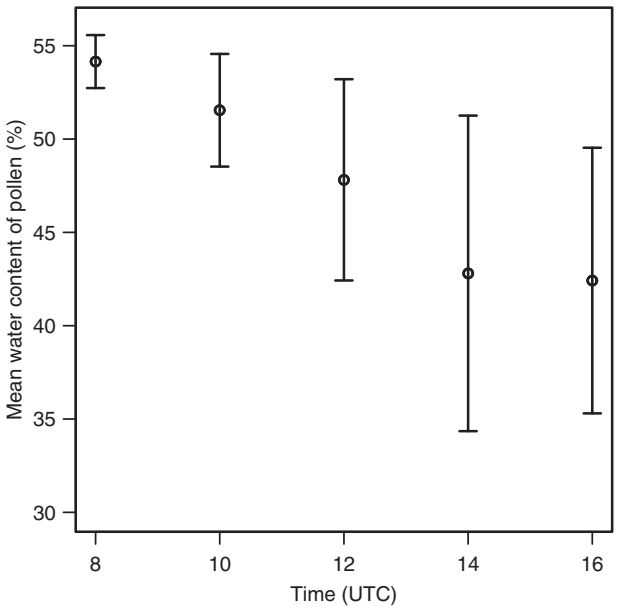

Fig. 1. Measured mean pollen water content at emission versus hour of emission. Points represent hourly means and bars represent hourly standard deviations calculated over the 23 days of experiments (2 years of experiments in Thiverval-Grignon).

3. Results

3.1. Modelling of pollen dehydration in the anthers throughout the day

The water content at the time of emission ranged from 26.5 to 56.2%. Fig. 1 represents the mean water content as a function of time of emission over the day. Over the 23 days of experimentations we observed that the later the emission after sunrise occurred the lower the mean of pollen water content was (Fig. 1). At 08:00 UTC, the measured mean water contents were the highest and fairly constant, around 54.1%. On the contrary, at 14:00 and 16:00 UTC, measured mean water contents were the lowest and the most variable between days. The decrease of water content is highly variable between days. These observations suggest that pollen dehydrates in the anther before being released.

Assuming that pollen dehydration in the anther is the result of its exposition to the air when anther opens, we estimated duration of dehydration, τ, for each water content measurement using the inverse function of Eq. (2) and assuming that VPD_t in the anther was equal to VPD_t measured at the top of the canopy. The estimated durations of dehydration were fairly stationary over the day although a high variability was observed. The median and standard deviation were 20 ± 9 min. No relationship between τ and mean climatic conditions was observed. We assumed that τ did not depend on climate or time of emission and fixed it at 20 min.

By setting $\tau = 20$ min in Eq. (2) we predicted the mean water content at emission. Fig. 2 shows the estimated mean water content as a function of emission time over six days of a single pollen emission period in 2009. The pollen water content follows the variation of vapour pressure deficit: the higher the increase of vapour pressure deficit over the day was, the higher the decrease of water content over the day was. Over the whole dataset, the estimations of pollen water content varied between 36 and 60% and the mean absolute error was 4%.

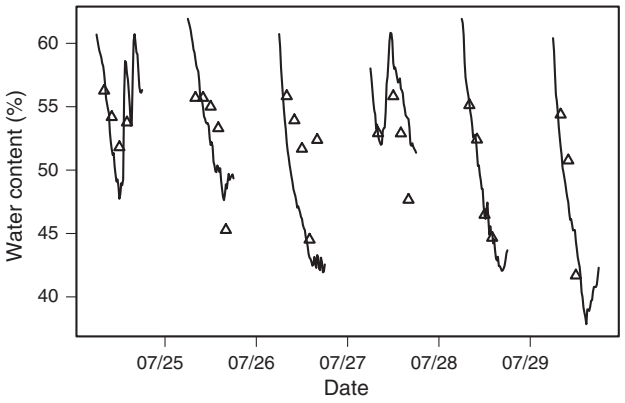

Fig. 2. Measured (triangle) and predicted (line) pollen water content as a function of time of pollen emission over a pollen emission period in 2009 in Thiverval-Grignon. Hourly variations of water content result from vapour pressure deficit variations.

3.2. Pollen dehydration results in a decrease of settling velocity and viability rate

3.2.1. Change of settling velocity distribution with pollen dehydration

In consequences to pollen dehydration over the day, we observed a decrease of pollen diameter and settling velocity over the day (Fig. 3). The effects of pollen dehydration on settling velocity distribution are clearly shown in Fig. 4. Its shows the measured settling velocity distributions for several classes of water content. The settling velocity distribution associated with the lowest class of water content corresponds to the pollen sample dried in the laboratory. For this sample, the mean settling velocity, mean water content and mean diameter were 19.2 cm s^{-1}, 87 μm and 6%.

Unimodal distributions were observed for water content higher than 54% or lower than 24%. In other cases, bimodal distributions were observed. For each class of water content, the associated distribution of settling velocity was adjusted by a sum of two Gaussian distributions (Eq. (3); mean R^2 = 0.99). Over all these adjusted distributions, the minimal 5% quantile was 16 cm s^{-1} and the maximal 95% quantile was 32 cm s^{-1}. For bimodal distribution, the mean threshold of settling velocity around which the two Gaussian distributions are split was 23 cm s^{-1}. The Gaussian distribution with a lower mean than 23 cm s^{-1} was referred as G1 and the other as G2. Estimated parameters of each Gaussian distribution are

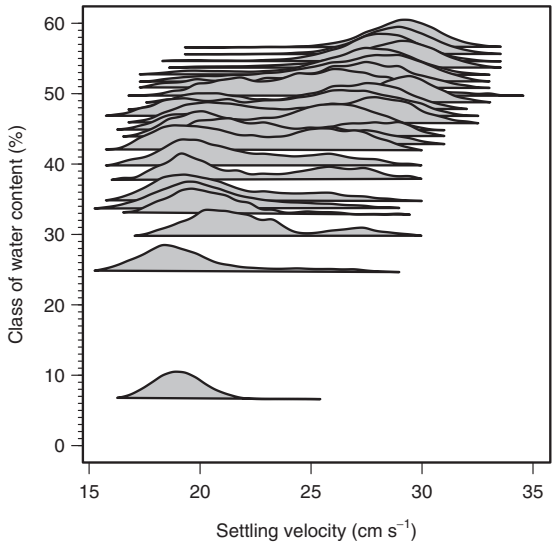

Fig. 4. Empirical settling velocity distributions versus classes of pollen water content. Settling velocity distributions are normalized by their maximal value to ensure that all distributions are visible, thus areas under the distributions are not comparable.

represented in Fig. 5. The proportion of G2 (A_2) increased linearly with mean water content (W_p in %) (Eq. (10); root mean squared error = 0.04). It was equal to 1, 0.5 and 0 for water content of 57.2, 41.6 and 26.1%, respectively (Fig. 5a).

$$A_2 = 0.0321W_p - 0.837 \quad (10)$$

Fig. 5b shows that the mode of G2 (μ_2 in cm s^{-1}) increased with water content (Eq. (11); root mean squared error = 0.5 cm s^{-1}) while the mode of G1 (μ_1 in cm s^{-1}) was more constant (Eq. (12); root mean squared error = 0.4 cm s^{-1}). Fig. 5c shows the regressions between water content and standard deviations of G1 and G2 (σ_1 and σ_2 in cm s^{-1}) given by Eqs. (13) and (14).

$$\mu_1 = 19 + \frac{20.7 - 19}{1 + \exp(-0.161(W_p - 40.93))} \quad (11)$$

$$\mu_2 = 24.7 + \frac{30 - 24.7}{1 + \exp(-0.165(W_p - 48.57))} \quad (12)$$

$$\sigma_1 = \min(1.178 + 0.015W_p, \quad 1.79) \quad (13)$$

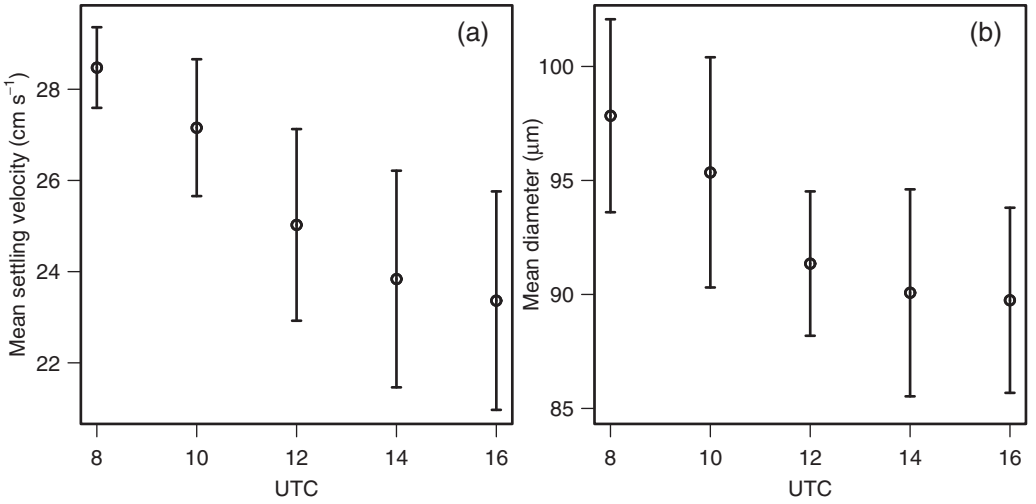

Fig. 3. Measured mean pollen settling velocity (a) and mean diameter (b) versus hour of emission. Points and bars represent hourly means and standard deviations calculated over 23 days (2 years of experiments in Thiverval-Grignon).

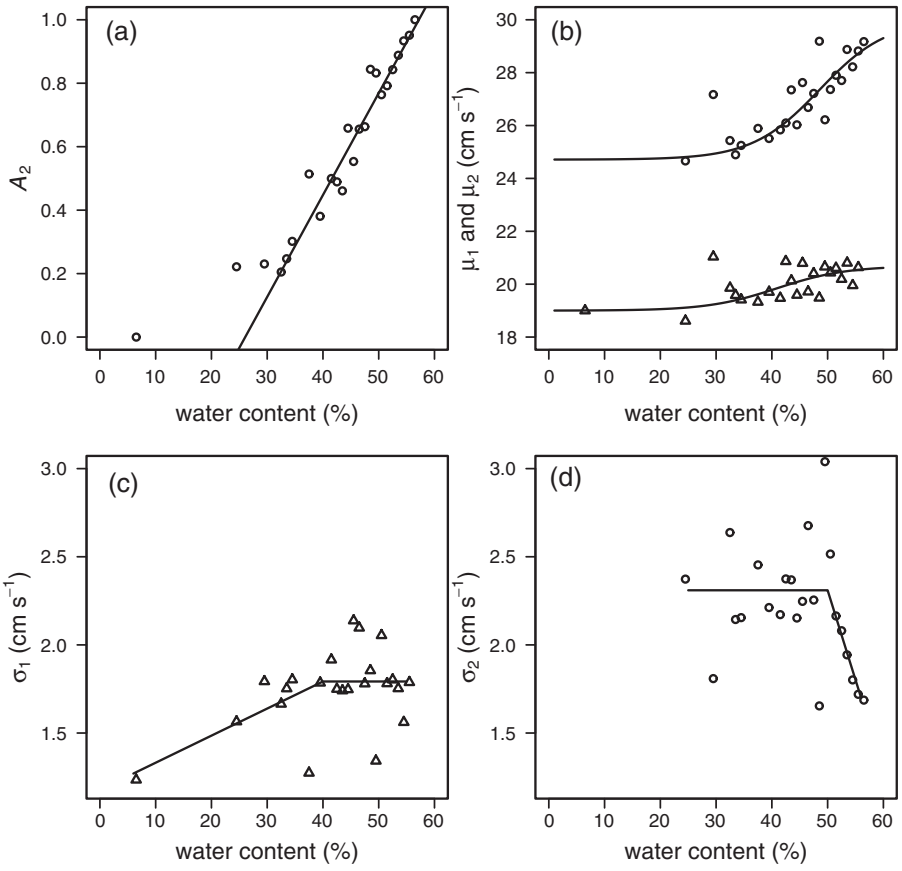

Fig. 5. Estimated parameters of the pollen settling velocity distributions versus classes of pollen water content. The distribution is a mixture of two normal distributions with five parameters μ_1, σ_1, μ_2, σ_2 and A_2. Parameters μ_1 and σ_1, represented on (b) and (c) with triangles, are the parameters of the first normal distribution with a mean lower than 23 cm s^{-1}. Parameters μ_2 and σ_2, represented on (b) and (d) with circle, are the parameters of the second normal distribution with a mean higher than 23 cm s^{-1}. Parameter A_2, represented in (a), is the area under the second normal distribution and $1 - A_2$ the area under the first normal distribution.

$$\sigma_2 = \min(7.39 - 0.102W_p, \quad 2.31) \tag{14}$$

To understand bimodal distributions of settling velocity, we investigated distributions of pollen diameter and shape. Pictures of pollen with different diameter and shape associated to contrasted water content are shown in Fig. 6. Highly hydrated pollen grains were large and spheroid (Fig. 6a) while highly dehydrated pollen grains were small and prismatic (Fig. 6c). For intermediate water content (Fig. 6b), pollen sample was composed of spheroid and prismatic. Nevertheless, we did not observe bimodal distribution of diameter which could explain alone bimodal distribution of settling velocity. On the contrary, distributions of kurtosis of grey intensity of individual pollen, K_p, were bimodal. Threshold of K_p around which pollen was either spheroid or prismatic was fixed at 0.75. The proportion of pollen with K_p higher than the threshold was highly correlated with the proportion of G2 ($r = 0.8$) suggesting that G2 was the settling velocity of spheroid pollen while G1 was the distribution associated with prismatic pollen. Therefore, bimodal distribution might be mainly explained with a change of shape (which also modify aerodynamics properties of the pollen) rather than a change of diameter.

3.2.2. Viable pollen has higher settling velocity than non-viable pollen

To relate settling velocity and viability by the use of water content, we proposed a theoretical relationship between settling velocity and water content for spheroid pollen grains. Theoretical settling velocity proposed here (Eqs. (4)–(6)) was calculated by setting $D_{ref} = 97.3$ μm and $W_{ref} = 55.6\%$. These parameters were calculated as the mean values of pollen samples supposed to be spheroid and defined by mean water content higher than 55%. In

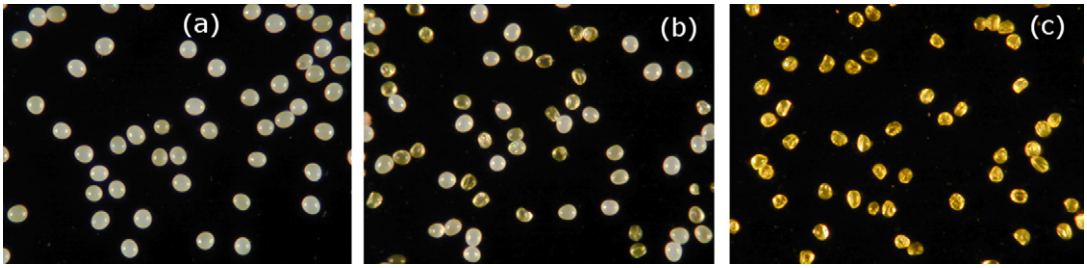

Fig. 6. Microscope photography of pollen sample with different mean water contents: 55 (a), 43 (b) and 30% (c). Pollen grains on (a) are spheroids while pollen grains on (c) are prismatic. On (b) pollen grains are either spheroid or prismatic.

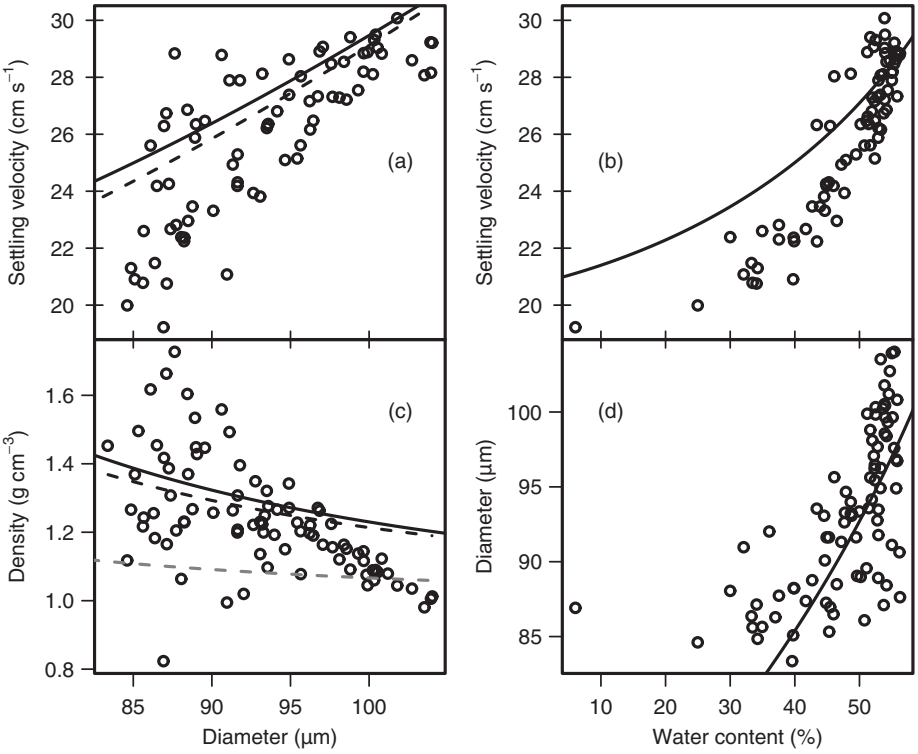

Fig. 7. Relationships between biophysical pollen characteristics: (a) settling velocity versus diameter, (b) settling velocity versus water content, (c) density versus diameter and (d) diameter versus water content. Points represent averages of measured biophysical variables for each pollen sample excepted for density. Density was calculated from averages of measured diameter and water content (Eq. (5)). Lines represent the following theoretical relationships. Theoretical settling velocity proposed by Aylor (2002; Eqs. (4) and (7) with D_{dry} = 78 μm) are represented by grey dotted line for ρ_{dry} = 1.14 g cm^{-3} and by black dotted line for ρ_{dry} = 1.45 g cm^{-3}. Black lines represent the theoretical relationships that we proposed with parameters m_{dry}, D_{ref} and W_{ref} equal to 0.266 μg, 97 μm and 55% (Eqs. (4)–(6)).

addition, the mean dry mass, m_{dry}, estimated from the pollen sample dried in the laboratory was 0.266 ± 0.008 μg.

To validate the theoretical relationships we compared then with the mean measurements of settling velocity, density, diameter and mean water content in each pollen sample collected during experiments located in Thiverval-Grignon. Fig. 7a and c shows settling velocity and pollen density as a function of diameter. When diameter increases, settling velocity decreases and density increases. The theoretical density proposed by Aylor (2002) with ρ_{dry} = 1.45 g cm^{-3} and the theoretical density proposed here were similar and were the more consistent with empirical density than theoretical density proposed by Aylor with ρ_{dry} = 1.14 g cm^{-3}. The similarity between these two theoretical relationships is also observed between settling velocities and diameter. Theoretical settling velocity was consistent with measurements for higher diameter than 95 μm while, for lower diameter, they overestimated measurements.

The relationship between mean diameter and mean water content is shown in Fig. 7d. Theoretical diameters proposed here (Eq. (6)) were consistent with measurements for water content higher than 40%. All diameters higher than 95 and 100 μm were associated with water content higher than 51 and 53%, respectively. For lower diameter, water content become highly variable between 6 and 55%. A general observation is that variability of mean value of settling velocity, density and diameter between pollen samples become high when diameter is lower than 95 μm. Probably, this pollen sample contains an important fraction of prismatic pollen for which projected diameters is inappropriate to reflect pollen characteristics.

Theoretical settling velocity as a function of water content proposed here (Fig. 7b) was consistent with measurements for the highest water contents but overestimated measurements in other cases. We explain this overestimation by the fact that the theoretical settling velocity is defined with the hypothesis of a spheroid pollen while pollen samples used to measure settling velocities contain more and more prismatic pollen when their water content decrease. More precisely, the fraction of spheroid pollen becomes lower than 0.5 for water content lower than 41.6% (Eq. (10)). At this water content, this hypothesis of spheroid shape becomes weak and could explain the large deviation between measured and theoretical settling velocities. Because prismatic pollen has lower settling velocity than spheroid pollen theoretical settling velocity becomes higher than measurements when water content decreases.

To estimate settling velocity distributions of viable and non-viable pollen, we calculated water content distribution associated with settling velocity distribution of spheroid pollen. First, from theoretical settling velocity calculated from water content (Eqs. (4)–(6)), we approximated the inverse relationship between settling velocity and water content by Eq. (15) (R^2 = 0.99).

$$W_p = I(v_S) = 88.52 - \frac{977,300}{v_S^{3.078}} \quad (15)$$

Second, assuming that G2 was the settling velocity distribution of spheroid pollen, we calculated water content distribution of spheroid pollen from settling velocity distribution G2 by a change of variable as formulated in Eq. (8). The water content distributions of spheroid pollen were skewed on the left. The mean varied between 35.3 and 56.7% and the quantiles 5 and 95% varied between 5–46% and 56–65%. The critical pollen water content that marks the change from spheroid to prismatic pollen shape was 25.6%. It was calculated from Eq. (15) and the settling velocity threshold between G1 and G2 equal to 23 cm s^{-1}. According to Eq. (9), the water content threshold under which pollen is dead

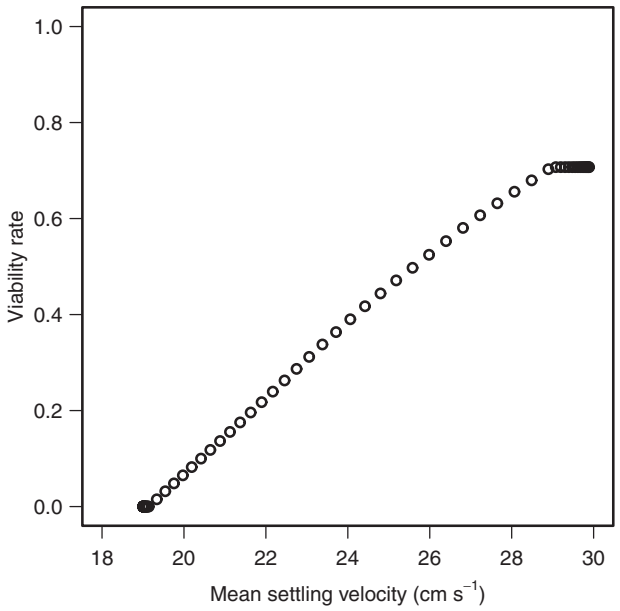

Fig. 8. Estimated viability rate versus mean settling velocity of pollen grains.

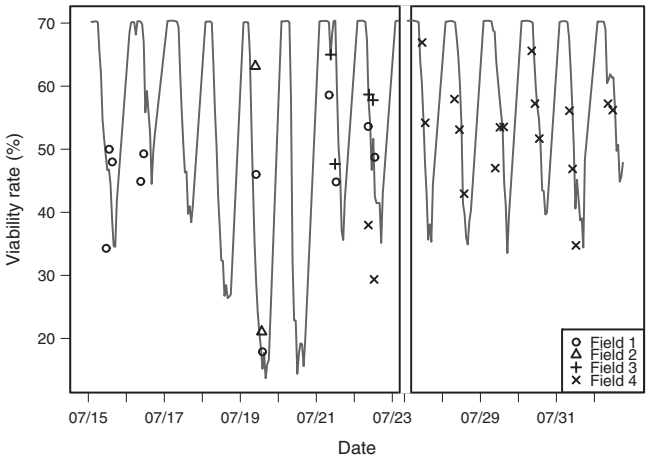

Fig. 9. Estimated viability rate per minute (grey line) and measured viability rate over 2–4 h periods (symbols) as a function of time of emission. Measurements were realized in 2010 near Beaufort-en-Vallée.

one, W_{dead}, was 30%, suggesting that prismatic pollen is non-viable. According to Eq. (15), W_{dead} corresponded to a settling velocity, $v_{s,dead}$, equal to 23.54 cm s^{-1}. Thus, proportion of potentially viable spheroid pollen corresponded to proportion of G2 higher than 23.54 cm s^{-1}.

For a given settling velocity distribution, the associated pollen viability rate was calculated as the fraction of spheroid pollen times the fraction of potentially viable spheroid pollen times an initial fraction of defective pollen. The proportion of potentially viable spheroid pollen was defined as the proportion of pollen with settling velocity higher than 23.54 cm s^{-1}. It varied between 0.68 and 1 over all measured settling velocity distributions. We estimated the initial rate of defective spheroid pollen to 0.71. It was estimated using Eq. (9) for water content of 57.2%, i.e., water content for which all pollen grains were spheroids. The viability rate calculated using settling velocity distribution was well correlated (0.97) with Eq. (9). Fig. 8 shows the relationship between viability rate of pollen and the mean value of bimodal distributions of settling velocity.

3.2.3. *Estimations of pollen viability rate in operational conditions have a good accuracy*

Fig. 9 represents measured viability rate for pollen emitted over a period of several hours and estimates viability rate per minute as a function of emission time. The measured viability rates are positioned in the figure at the middle of the exposure period. We proposed a fixed estimation for four fields with different hybrid varieties. The decreasing viability rate within the day is well reproduced by the model particularly on July 19 when a high vapor pressure deficit occurs. The model has a good accuracy given the mean absolute error equal to ± 9.8 percentage points.

3.3. *The decrease of air humidity throughout the day decrease cross-pollination risks*

Consequently to pollen dehydration in anthers as a function of VPD of the air, settling velocity and viability rate decrease. Fig. 10 shows the predictions of viability rate and the mean settling velocity of viable pollen at emission time as a function of VPD conditions. For high VPD, the viability rate could be drastically reduced at emission time until 0.2 while the mean settling velocity of viable pollen decreased from 30 to 25 cm s^{-1}.

To study the effect of vapour pressure deficit on pollen dispersal, we calculated pollen water content and associated settling

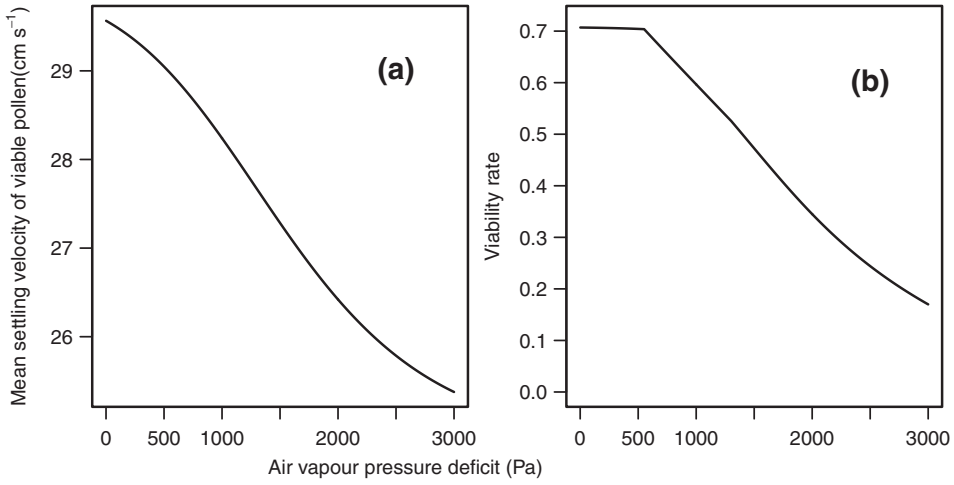

Fig. 10. Estimation of mean settling velocity of viable pollen (a) and viability rate (b) at emission time as a function of vapour pressure deficit of the air. These estimations were calculated using the model that we developed.

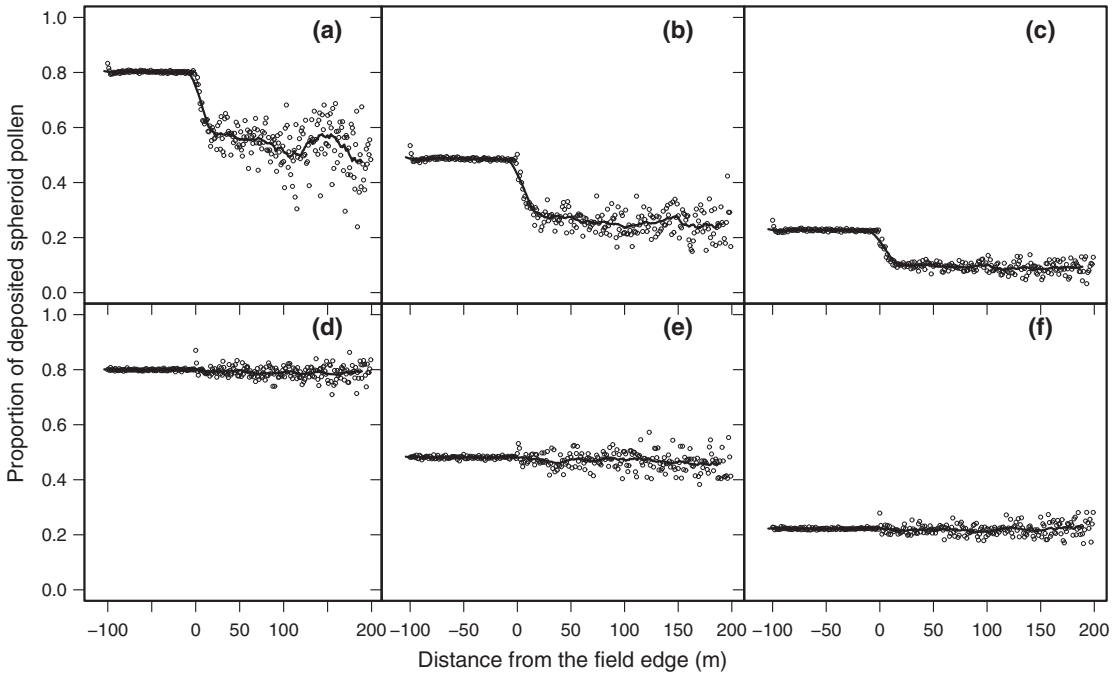

Fig. 11. Proportion of partially viable spheroid pollen within deposited pollen on the ground versus distance from the edge of the maize field. Points are the simulations while lines are a moving average. The three graphs on the first row ((a), ((b) and (c)) represent simulations for wind speed equal to 1 m s^{-1} and those on the second row ((d), (e) and (f)) represent simulations for wind speed equal to 5 m s^{-1}. For each column, the two graphs represent simulations for the same vapour pressure deficit conditions which are equal to 1100 ((a) and (d)), 2200 ((b) and (e)) and 3300 Pa ((c) and (f)).

velocity distribution of dead pollen, i.e., prismatic, and partially viable pollen, i.e., spheroid for contrasted vapour pressure deficit. These settling velocity distributions were used, as input, to simulate pollen dispersal for two conditions of wind speed. For vapour pressure deficits of 1100, 2200 and 3300 Pa, we estimated mean water content at emission of 51, 41 and 33%, respectively. The associated parameters of the sum of bi-Gaussian distribution (Eq. (3)) were equal to $\{\mu_1 = 20.4 \pm 1.75\,\mathrm{cm\,s^{-1}}$, $A_2 = 0.79$, $\mu_2 = 27.8 \pm 1.70\,\mathrm{cm\,s^{-1}}\}$, $\{\mu_1 = 19.8 \pm 1.75\,\mathrm{cm\,s^{-1}}$, $A_2 = 0.47$, $\mu_2 = 25.9 \pm 2.25\,\mathrm{cm\,s^{-1}}\}$ and $\{\mu_1 = 19.4 \pm 1.75\,\mathrm{cm\,s^{-1}}$, $A_2 = 0.22$, $\mu_2 = 25.1 \pm 2.25\,\mathrm{cm\,s^{-1}}\}$. Fig. 11 represents the proportion of partially viable spheroid pollen relatively to total pollen deposited on the ground as a function of distance from the crop for two wind speeds and three vapour pressure deficits. For wind speed of 5 m s^{-1}, the rate of spheroid pollen deposited at various distance from the crop was similar to the rate at emission. On the contrary, for wind speed of 1 m s^{-1}, the rate of spheroid pollen deposited varied as a function of distance from the crop. In the crop, rate of spheroid pollen were slightly higher than emission rate. Downwind from the crop, simulations revealed a decrease of spheroid pollen rate. This decrease was observed during the 21 m until equilibrium was reached. Due to higher settling velocity, partially viable spheroid pollen travelled lower distance than non-viable prismatic pollen.

4. Discussion

4.1. Comparison of experimental measurements with published literature data

Pollen water content measured at emission time varied from 25 to 56%, which was consistent with measurements made by Aylor (2002) who found a range of 40–56%. The maximal water content was 56%, which is close to the lower boundary of the range observed in the literature: 55–60% (Kerhoas et al., 1987; Roeckel-Drevet et al., 1995; Fonseca and Westgate, 2005). This could be explained by the fact that this value corresponded to a pollen sample collected at 08:00 UTC while emission could have started as early as 06:00 UTC (around 2 h after sunrise (Marceau et al., 2011)); pollen collected at 08:00 UTC had most likely begun to dehydrate and water content at this time was not maximal. The lowest water content was 6%, measured for the pollen sample dried in the laboratory. Aylor et al. (2003) suggested that pollen water content reaches an equilibrium state with air as a function of relative humidity conditions and thus reaches values close to 0% only when air is highly dry.

Highest mean diameter measured here was 104 μm, which is consistent with measurements made by Aylor (2002) but higher than those of van Hout and Katz (2004) who found 93 μm. However, for the highest hydrated pollen samples collected here, mean water content was 55.6% and mean diameter was 97 μm notably lower than 104 μm. Using the density given by Aylor (2002) for highly hydrated grains, 1.2 g cm^{-3}, and Eq. (5) to calculate pollen mass using water content, we obtained a volume-equivalent diameter of 98, 99 and 102 μm for water content of 55, 56 and 60%, respectively. Knowing that we did not measured water contents higher than 56%, we assume that the measured diameter of 104 μm is an extreme value, probably due to the sampling: it is not fully representative of the pollen grains diameter. In addition, we observed that diameters were highly variable for high water contents. The lowest mean diameter measured here was 83 μm, slightly higher than measurements of Aylor (2002) and van Hout and Katz (2004) who found ~78 μm. For pollen sample dried in the laboratory, mean diameter was 87 μm. Because dried pollen grains are not spheroid but are multi-faced prisms, the measured projected diameter largely depends on which face the pollen is disposed on the microscopic slide inducing a large variability. Due to high variability observed for prismatic and spheroid pollen grains, we recommend the use of a sufficient number of pollen grains probably higher than 300 grains.

Density has been observed to increase when diameter decreases. This is the result of pollen dehydration due to water density lower than dry density. We tested the ability of dry pollen density

proposed by Aylor (2002) and van Hout and Katz (2004), as a parameter of Eq. (7), to accurately estimate density and settling velocity and found that the first one is most consistent with our data. In addition, the theoretical settling velocity proposed by Aylor (2002), with ρ_{dry} equal to 1.45 g cm^{-3}, and the calculation based on our formulation, provided similar results also consistent with the measurements.

4.2. A contribution to the understanding of pollen dehydration in the anther

We proposed a simple way to estimate mean water content of pollen at emission assuming that pollen grains dehydrate in the dehiscent anther. The water content was calculated as a function of air vapour pressure deficit using the model of Fonseca and Westgate (2005) and setting a constant duration of dehydration of 20 min estimated from our measurements. This assumes that the variations of pollen water content result from diurnal changes of air vapour pressure deficit.

However, our estimations of pollen water content at emission had a low accuracy ($R^2 = 0.49$). Most likely, the vapour pressure deficit conditions in the anther are different than those in the air due to, for example, radiations intercepted by anthers and humidity saturation within the anther. Further investigation on pollen dehydration within anthers should consider factors affecting microclimatic conditions within anthers. In addition, the initial water content in the model of dehydration of Fonseca and Westgate (2005) was equal to 63%, which appears to be high in comparison to the literature (between 55 and 60%; Kerhoas et al., 1987; Roeckel-Drevet et al., 1995; Fonseca and Westgate, 2005). Our measurements did not provide information on initial pollen water content, just after anther dehiscence, enabling to determine which value is the more relevant. An investigation of initial water content and more generally of initial biophysical characteristics of pollen should be helpful to study pollen dehydration in the anthers.

We used the model of Fonseca and Westgate (2005) to estimate duration of pollen dehydration in the anther. Because of the uncertainty in initial water content and the use of air vapour pressure deficit in the air rather than in the anther, the duration of dehydration was most likely roughly estimated. Duration of dehydration represents the duration between anther dehiscence and effective pollen release including the time needed for anther to enlarge its pore enough for pollen extraction. In our study we do not found any relation between meteorological conditions and duration of dehydration while Keijzer et al. (1996) suggested that the rate of pore enlarging increases with vapour pressure deficit. Moreover, wind speed enhances the extraction of pollen by shaking anthers and tassels (Urzay et al., 2009), which theoretically leads to reduce the duration of dehydration. In our opinion, the estimations of duration of dehydration used here do not allow to observe these effects. By taking into account for anthers moisture conditions and using accurate initial water content, we suppose that the inverse modelling method proposed here could highlight meteorological effects on duration of dehydration.

4.3. Changes in pollen shape and viability in response to pollen dehydration

We can distinguish two phases during pollen dehydration: in the first phase, pollen deflates with keeping spheroid shape and the diameter remains proportional to its volume; during the second phase, depressions appear on pollen surface until it looks like a “deflated balloon”. This loss of spheroid shape, probably due to membrane rigidity, results in the fact that the volume is no longer proportional to the cubic power of equivalent diameter. In this study, the mean water content that marks the change from spheroid to prismatic pollen shape was estimated at 27%. It was calculated from the bimodal settling velocity distributions as the water content corresponding to the settling velocity threshold between the two distributions. Similar critical water contents have been reported by Fonseca and Westgate (2005) who observed that when water content dropped below 30% pollen was non-viable and by Kerhoas et al. (1987) who observed that when water content dropped below 28% irreversible alterations of membrane permeability and of pollen physiology happened. We are wondering if these correlated effects are physiologically linked. Roeckel-Drevet et al. (1995) proposed two hypotheses for viability loss: (i) the difficulty of the pollen to rehydrate and become turgescent or (ii) the difficulty of the dry pollen to resume its metabolism after rehydration. They gave several elements to support each of them and they concluded that the two hypotheses might be valid. Whatever the mechanism of viability loss, pollen grains are tolerant to dehydration until critical water content (Nepi et al., 2010). Obviously the critical water content for pollen viability loss, and potential dependency to variety, require more specific investigations.

Projected diameter has been suggested as a mean to investigate settling velocity (Aylor, 2002). Given the change in shape observed here, projected diameter would not be a good indicator of prismatic pollen volume and in turn of water content and settling velocity. We observed that when diameter was lower than 95 μm, its relationships with settling velocity, density and water content become highly variable (Fig. 7). On the contrary, water content has been observed to be a good indicator of mean settling velocity (Fig. 7) and settling velocity distributions (Fig. 4). The theoretical settling velocity of spheroid pollen is higher than measured mean settling velocity of pollen sample collected during Thiverval-Grignon location experiments. Most likely, this is explained by the fact that pollen samples not only contained spheroid but also prismatic pollen which have a lower settling velocity than spheroid pollen.

4.4. The higher settling velocity of partially viable relatively to non-viable pollen leads to reduce cross-pollination risks under low wind speeds

Simulations of pollen dispersal when wind speed is low revealed a gradient of spheroid pollen deposited downwind from the crop. On the contrary, when wind speeds are high, no gradient are simulated. In our opinion, when wind speeds are high the role of settling velocity on vertical pollen movement is negligible relatively to vertical turbulent fluctuations. In this case, trajectory of prismatic and spheroid are mainly determined by wind characteristics. When wind speeds decrease, vertical turbulent fluctuations decrease and settling velocity become less and less negligible. Thus, for low wind speed, spheroid pollen drops faster on the ground than non-viable prismatic pollen due to higher settling velocity which reduced the quantity of viable pollen for distance higher than 20 m (Fig. 11). By taking into account different settling velocity distributions for viable and non-viable pollen grains we simulated a gradient of viability which is an original result. We suggest accounting for these different settling velocity distributions to simulate more accurately cross-pollination using physically based models.

4.5. Bimodal distribution of settling velocity as a proxy to estimate pollen characteristics

In our study, the distribution of settling velocity was observed as a bimodal one due to spheroid and prismatic pollen shapes instead of large and small pollen sizes. We used the measurements of settling velocity distribution to estimate (i) the fraction of spheroid and prismatic pollen, (ii) the critical water content which marks the change between spheroid to prismatic pollen shape (iii) the

distribution of water content of spheroid pollen as well as (iv) the pollen viability rate.

The settling velocities of spheroid pollen were higher than those of prismatic pollen. Settling velocities of spheroid pollen were sensitive to water content variations: when mean water content decreased mean settling velocity of spheroid pollen decreased. For spheroid pollen grains we proposed a theoretical relationship between settling velocities and water content. We used it to estimate water content distribution of spheroid pollen from their settling velocity distribution. We assumed that a given settling velocity was related to a unique water content. Nevertheless, the variability of dry mass, diameter or shape most likely involved variability in settling velocity unrelated to water content. This natural variability would have to be investigated further to improve estimation of water content distribution.

For prismatic pollen, we observed that their settling velocities distributions were the lowest and clearly distinct from settling velocities distribution of spheroid pollen. This distinction was most likely induced by their different aerodynamical properties. In addition, settling velocities of prismatic pollen were fairly stationary relative to settling velocities of spheroid pollen. Water content of prismatic pollen varied from 27% (the estimated transition from spheroid to prismatic shapes) to 6% (the lowest measured mean water content) corresponding to water mass varying from 0.29 to 0.36 μg. These low variations of water mass (in comparison mass water of spheroid pollen ranged between 0.36 and 0.61 μg) probably explain the fairly stationary settling velocity. We did not estimate water content distribution of prismatic pollen from settling velocity distributions due to unknown relationship for prismatic pollen between settling velocity and water content.

We proposed a way to calculate viability rate from settling velocity distribution based on the critical water content of 30% found in the literature under which pollen becomes non-viable (Fonseca and Westgate, 2005). We found that the prismatic pollen was associated with lower water content than 27% suggesting that prismatic pollen was non-viable. On the contrary, spheroid pollen grains were partially viable depending on the fraction with water content higher than 30%. To easily estimate this fraction we calculated the settling velocity associated to water content of 30% and found 23.54 cm s^{-1}. Thus the fraction of settling velocity of spheroid pollen higher than 23.54 cm s^{-1} provides the fraction of spheroid viable pollen. Moreover, we used an initial fraction of defective pollen according to authors who always observed a non-viable fraction of pollen (Fonseca and Westgate, 2005; Roeckel-Drevet et al., 1995). This initial fraction of defective pollen was estimated for one hybrid maize varieties. This estimation seems robust for hybrid varieties showing the accuracy of viability rate estimations for four different hybrid maize varieties. However, this parameter could be significantly different for inbred lines or population and require further investigations (Aylor et al., 2005).

5. Conclusion

Our work was dedicated to the estimation of viability rate and settling velocities distributions at emission time taking into account pollen dehydration in the anther. Our results show that viability rate and settling velocity at emission time decrease throughout the day depending on the time course of vapour pressure deficit. This suggests that fertilization could be reduced during warm periods leading to reduce kernel or seed productions.

Our work is a contribution to biophysical modelling of cross-pollination. The model was validated with success for hybrid varieties in operational conditions (meteorological data recorded in a distant station on a hourly basis). However, further investigations are required to extend these results for maize population or inbred lines. Based on the new knowledge on biophysical characteristics presented here and total emission previously proposed (Marceau et al., 2011), simulations of cross-pollination risks using a physically based model of dispersal are now possible taking into account fluctuation of meteorological conditions. To finish, associated with further work such as modelling the biological process of silks emission and viability, our biophysical approach could be useful to simulate gene flows.

Acknowledgement

The present work was funded by Arvalis - Institut du vegetal. We also thank Terrena for support during Beaufort-en-Vallée location experiments. Brigitte Durand provided excellent technical assistance and we are indebted for her personal involvement in this work. We also thank Jessica Bertheloot, Bruno Andrieu for reviewing and helpful discussion as well as Martin Cellier for technical assistance. Lastly, we would like to thank Suzette Tanis-Plant for fruitful discussions in English and the reviewers for their valuable comments.

References

Arritt, R.W., Clark, C.A., Goggi, A.S., Sanchez, H.L., Westgate, M.E., Riese, J.M., 2007. Lagrangian numerical simulations of canopy air flow effects on maize pollen dispersal. Field Crops Res. 102, 151–162.
Aylor, D.E., 2002. Settling speed of corn (*Zea mays*) pollen. J. Aerosol Sci. 33, 1601–1607.
Aylor, D.E., 2003. Rate of dehydration of corn (*Zea mays* L.) pollen in the air. J. Exp. Bot. 54, 2307–2312.
Aylor, D.E., 2004. Survival of maize (*Zea mays*) pollen exposed in the atmosphere. Agric. Forest Meteorol. 123, 125–133.
Aylor, D.E., Baltazar, B.M., Schoper, J.B., 2005. Some physical properties of teosinte (*Zea mays* subsp *parviglumis*) pollen. J. Exp. Bot. 56, 2401–2407.
Aylor, D.E., Schultes, N.P., Shields, E.J., 2003. An aerobiological framework for assessing cross-pollination in maize. Agric. Forest Meteorol. 119, 111–129.
Beckie, H.J., Hall, L.M., 2008. Simple to complex: modelling crop pollen-mediated gene flow. Plant Sci. 175, 615–628.
Di-Giovanni, F., Kevan, P.G., Nasr, M.E., 1995. The variability in settling velocities of some pollen and spores. Grana 34, 39–44.
Dupont, S., Brunet, Y., Jarosz, N., 2006. Eulerian modelling of pollen dispersal over heterogeneous vegetation canopies. Agric. Forest Meteorol. 141, 82–104.
Fonseca, A.E., Westgate, M.E., 2005. Relationship between desiccation and viability of maize pollen. Field Crops Res. 94, 114–125.
Hatfield, J.L., Baker, J.M., 2005. Micrometeorology in Agricultural Systems. Agronomy Monograph No. 47, Madison, Wisconsin, USA.
Jarosz, N., 2003. Etude de la dispersion atmosphérique du pollen de maïs: Contribution à la maitrise des risques de pollinisation croisée. AgroparisTech-INRA, Paris, p. 128.
Jarosz, N., Loubet, B., Durand, B., Foueillassar, X., Hubert, L., 2005. Variations in maize pollen emission and deposition in relation to microclimate. Environ. Sci. Technol. 39, 4377–4384.
Jarosz, N., Loubet, B., Huber, L., 2004. Modelling airborne concentration and deposition rate of maize pollen. Atmos. Environ. 38, 5555–5566.
Keijzer, C.J., LeferinkTenKlooster, H.B., Reinders, M.C., 1996. The mechanics of the grass flower: anther dehiscence and pollen shedding in maize. Ann. Bot. 78, 15–21.
Kerhoas, C., Gay, G., Dumas, C., 1987. A multidisciplinary approach to the study of the plasma-membrane of *Zea mays* pollen during controlled dehydration. Planta 171, 1–10.
Loubet, B., Jarosz, N., Saint-Jean, S., Huber, L., 2007. A method for measuring the settling velocity distribution of large biotic particles. Aerobiologia 23, 159–169.
Luna, S., Figueroa, J., Baltazar, B., Gomez, R., Townsend, R., Schoper, J.B., 2001. Maize pollen longevity and distance isolation requirements for effective pollen control. Crop Sci. 41, 1551–1557.
Marceau, A., Loubet, B., Andrieu, B., Durand, B., Foueillassar, X., Huber, L., 2011. Modelling diurnal and seasonal patterns of pollen emission in relation to meteorological conditions. Agric. Forest Meteorol. 151, 11–21.
Nepi, M., Cresti, L., Guarnieri, M., Pacini, E., 2010. Effect of relative humidity on water content, viability and carbohydrate profile of *Petunia hybrida* and *Cucurbita pepo* pollen. Plant Syst. Evol. 284, 57–64.
Nepi, M., Franchi, G.G., Pacini, E., 2001. Pollen hydration status at dispersal: cytophysiological features and strategies. Protoplasma 216, 171–180.
Rasband, W.S., 1997–2009. ImageJ. U.S. National Institutes of Health, Bethesda, Maryland, USA, http://rsb.info.nih.gov/ij/.
Roeckel-Drevet, P., Digonnet, C., Matthysrochon, E., Champiat, D., Dumas, C., 1995. Fertility of *Zea mays* pollen during dehydration – physiological steps outlined by nucleotide measurements. Plant Physiol. Biochem. 33, 289–294.

Saint-Jean, S., Chelle, M., Huber, L., 2004. Modelling water transfer by rain-splash in a 3D canopy using Monte Carlo integration. Agric. Forest Meteorol. 121, 183–196.
Saint-Jean, S., Testa, A., Kamoun, S., Madden, L.V., 2005. Use of a green fluorescent protein marker for studying splash dispersal of sporangia of *Phytophthora infestans*. Eur. J. Plant Pathol. 112, 391–394.
Shivanna, K.R., Heslopharrison, J., 1981. Membrane state and pollen viability. Ann. Bot. 47, 759–770.
Urzay, J., Smith, S.G.L., Thompson, E., Glover, B.J., 2009. Wind gusts and plant aeroelasticity effects on the aerodynamics of pollen shedding: a hypothetical turbulence-initiated wind-pollination mechanism. J. Theor. Biol. 259, 785–792.
van Hout, R., Katz, J., 2004. A method for measuring the density of irregularly shaped biological aerosols such as pollen. J. Aerosol Sci. 35, 1369–1384.
Viner, B.J., Arritt, R.W., 2010. Increased pollen viability resulting from transport to the upper boundary layer. Field Crops Res. 119, 195–200.
Viner, B.J., Westgate, M.E., Arritt, R.W., 2010. A model to predict diurnal pollen shed in maize. Crop Sci. 50, 235–245.
Westgate, M.E., Boyer, J.S., 1986. Reproduction at low silk and pollen water potentials in maize. Crop Sci. 26, 951–956.